Acta Oceanol. Sin., 2019, Vol. 38, No. 8, P. 94–100
https://doi.org/10.1007/s13131-019-1426-2
http://www.hyxb.org.cn
E-mail: hyxbe@263.net

An improved frequency shift method for ATI-SAR flat earth phase removal

Yubin Zhang[1, 2], Jie Zhang[1], Junmin Meng[1], Chenqing Fan[1]*

[1] First Institute of Oceanography, Ministry of Natural Resources, Qingdao 266061, China

[2] College of Information Science and Engineering, Ocean University of China, Qingdao 266100, China

Received 4 May 2018; accepted 19 June 2018

Abstract

An improved frequency shift method is proposed to remove the flat earth phase in ATI-SAR ocean surface motion detection in this study. First, two conventional flat earth effect removal methods (i.e., the frequency shift method and the orbital parameter method) are introduced and compared. Then, two improvements to frequency shift method are suggested. In the first improvement, the phase diagram is divided into several sub-blocks to calculate the phase fringe frequency. In the second improvement, a function between the phase of land regions and position is fitted to correct the residual flat earth phase based on the phase of the land regions that tend toward zero in an along-track interferogram. It is found that the improved frequency shift method is greatly improved; and it agrees well with the orbital parameter method, and achieves similar accuracy.

Key words: flat earth phase, ATI-SAR, frequency shift, orbital parameter

Citation: Zhang Yubin, Zhang Jie, Meng Junmin, Fan Chenqing. 2019. An improved frequency shift method for ATI-SAR flat earth phase removal. Acta Oceanologica Sinica, 38(8): 94–100, doi: 10.1007/s13131-019-1426-2

1 Introduction

Synthetic aperture radar interferometry (InSAR) is the combination of interferometry technology and synthetic aperture radar (SAR) (Rosen et al., 2000). InSAR generally utilizes at least two apertures to repeatedly image the same region of earth surface, obtains two images with high inter-image coherence (Bamler and Hartl, 1998), and retrieves valuable information from their interferometric phase. InSAR can be classified as across-track interferometric (XTI) SAR and along-track interferometric (ATI) SAR: the former observes topography (Rosen et al., 2000; Bamler and Hartl, 1998), while the latter observes ocean surface currents (Romeiser et al., 2010, 2014).

The interferometric phase is the phase difference between two coherent complex images, and includes two parts: one is attributed to the elevation or slant range displacement, and the other is attributed to the flat earth effect. If the flat earth effect is not considered, points with the same elevation and zero speed should have the same phase. However, in practice, the phase appears different offset with positions due to the geometric relationship between the SAR apertures and the ground targets, leading to a periodic spatial distribution phase called the flat earth effect (Rosen et al., 2000; Bamler and Hartl, 1998; Zebker et al., 1997). As the dominant part of the original interferometric phase, the flat earth phase overshadows the variations of the ocean surface currents or topography. Therefore, it is necessary to remove the flat earth phase to retrieve the pertinent information. In addition, the precision of the flat earth phase affects the retrieval precision, and the flat earth phase removal contributes to phase unwrapping because it reduces the phase fringe density.

Two main methods are used to remove flat earth phase. The orbit parameters method utilizes satellite orbital parameters and the longitude and latitude of the image to calculate the flat earth phase (Ai and Li, 2009; Geudtner and Schwäbisch, 1996; Cao et al., 2013). The orbital parameters method can remove the flat earth phase accurately when the orbital parameters are sufficiently precise. However, when the parameters are incomplete or imprecise, this advantage will be suppressed (Kimura and Todo, 1997; Kohlhase et al., 2003). The frequency shift method removes the flat earth phase by estimating the fringe frequency of an interferogram and making circular frequency shifts (Wang et al., 2004; Gatelli et al., 1994; Moreira et al., 1995; Peng et al., 2009). The frequency shift method removes the flat earth phase based solely on the interferogram, it does not require any additional parameters; however, its relatively low accuracy can cause inaccurate retrieval of topography, ocean surface current, or other desirable information.

This paper suggests some improvements to the frequency shift method to improve the precision of ATI data from the TanDEM-SAR satellites formation. The remainder of this paper is organized as follows. A detailed description of data is given in Section 2. In Section 3, two conventional flat earth effect removal methods are introduced and their results are compared. In Section 4, two improvements to the frequency shift method are proposed and the results are discussed.

2 Data

The ATI complex data sets stem from TanDEM-X satellites formation, which was developed by Germany and is composed of the TerraSAR-X satellite (launched in June 2007) and its companion TanDEM-X (launched in June 2010) (Suchandt and Runge,

Foundation item: The National Key Research and Development Program of China under contract No. 2016YFC1402703; the National Natural Science Foundation of China under contract Nos 61471136 and 61501130.
*Corresponding author, E-mail: fanchenqing@fio.org.cn

2015). This satellite formation system's primary mission is to measure global digital elevation (Krieger et al., 2007); however, by performing baseline adjustment, ocean surface currents can also be measured (Romeiser et al., 2014). The instruments on both satellites are advanced high resolution X-band SARs that can be operated in Spotlight, Stripmap, and ScanSAR modes with full polarization capabilities (Krieger et al., 2007; Stangl et al., 2006). The center frequency of the instruments is 9.65 GHz, and they feature a selectable SAR chirp bandwidth of up to 300 MHz. Interferometric data can be acquired in (1) pursuit monostatic mode, in which both satellites are operated independently, (2) bistatic mode, in which one satellite serves as the transmitter and both satellites record the scattered signal simultaneously, and (3) alternating bistatic mode, in which the transmitter changes from pulse to pulse.

The satellites feature a tracking, occultation, and ranging instrument package that includes a dual-frequency GPS tracking receiver and a laser reflector set for high-precision orbit determination and occultation measurements, supporting high-precision orbit determination with an accuracy exceeding 20 cm (Werninghaus and Buckreuss, 2010; Yoon et al., 2009). Such accurate orbital information ensures the high accuracy of the orbital parameter method for flat earth effect removal.

As shown in Fig. 1, the interferometric data sets analyzed in this study were acquired at the Orkney Islands north of the mainland of Scotland on March 19, 2012, and imaged in Stripmap mode with VV polarization. All the scenes have a nominal incidence angle of 31° and a full resolution pixel spacing on the order of 1.7 m×2.1 m (range×azimuth). The effective AT baseline is 40.27 m and the effective XT baseline is approximately 24 m. To reduce the amount of calculation required, only the area in the red box in the right image is processed.

3 The conventional methods for flat earth phase removing

There are two primary conventional methods for removing flat earth phase. One is called frequency shift method; this method estimates the fringe frequency of an interferogram and performs circular frequency shifts. The other is called the orbital parameters method; this method utilizes the orbital parameters of the InSAR satellite and the longitude and latitude of the image to calculate the flat earth phase. The details of these two methods are described in the following subsections.

3.1 *Frequency shift method*

The frequency shift method removes the flat earth phase based solely on the interferogram and it does not require any additional parameters. When no flat earth effect is present, the spatial frequency of the phase fringe (i.e., the frequency spectrum peak value of the interferogram) should be zero (Ai and Li, 2009; Gatelli et al., 1994). Therefore, after performing a Fourier transform of the interferogram, the flat earth phase can be removed by searching for the frequency peak value and shifting it to zero using a circular shifting method. The two-dimensional interferogram needs to remove the flat earth phase along both the row and column directions.

Assume the master and slave images after registration are $M(m,n)$ and $S(m,n)$, respectively. The interferogram is $I(m,n) = M(m,n) \cdot S^*(m,n)$, and the two-dimensional interferometric phase is $\varphi(m,n) = \arg(I(m,n))$. Here, the asterisk * indicates the conjugate complex, arg( ) calculate the argument, and m and n are the row and column coordinates in the image coordinate system, respectively. Generally, the interferogram phase changes periodically along the range and azimuth directions. Therefore, processing along both the row and column directions may be necessary. Because both directions involve the same processing steps, row processing, which is the range direction in the data used in this paper, will be described next as an example.

(1) Calculating the frequency spectrum peak value of the phase fringe

First, the two-dimensional phase is transformed to the frequency domain by a one-dimensional fast Fourier transform (FFT) row by row. The values are then summed column by column, resulting in a one-dimensional array that corresponds to the rows. The position of the maximum value of this one-dimensional array corresponds to the approximate frequency spectrum peak value f_1 in the row direction.

To obtain a more accurate frequency, a high-order smooth interpolation such as the cubic spline method is applied to the 5 points centered on the maximum value of the one-dimensional array. Then, the 5-point interval is interpolated into 400 grid points here. The position of the maximum value of interpolated results corresponds to the exact frequency spectrum peak value f_2. The phase corresponding to f_2 is the flat earth phase, which can be described as follows:

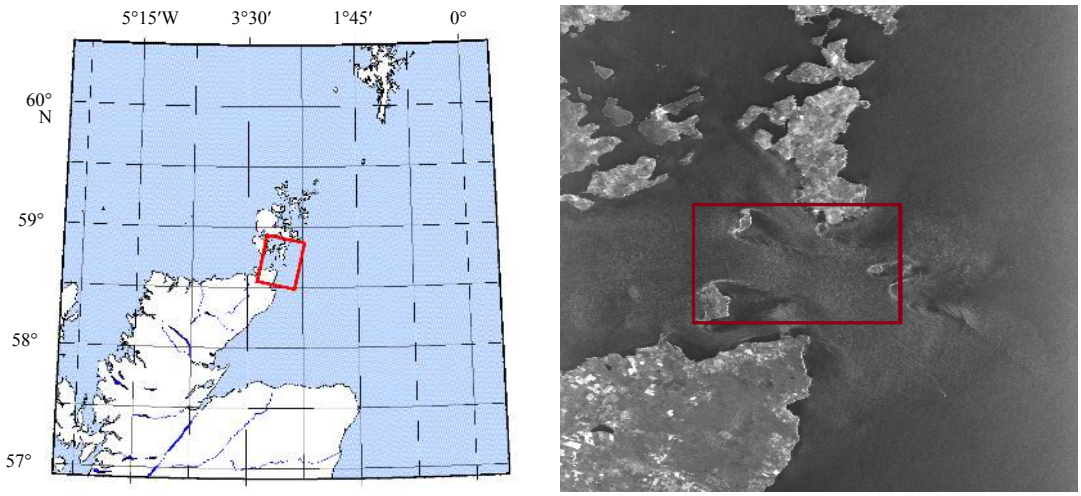

Fig. 1. Schematic diagram of the study area.

$$\varphi_f(n) = \arg(\exp(j2\pi f_2 n)), \tag{1}$$

where n indicates the column number of a resolution unit within a row, and j is the imaginary unit.

(2) Removing the flat earth phase

To remove the flat earth effect, the interferogram is multiplied by the phase shift factor corresponding to f_2:

$$\varphi'(m,n) = \arg(I(m,n) \cdot \exp(-\mathrm{j}2\pi f_2 n)), \tag{2}$$

where $\varphi'(m,n)$ indicates the interferometric phase after removing flat earth phase.

3.2 *Orbital parameters method*

When two apertures S_1 and S_2 successively image the target point P, the phase difference ϕ_f corresponding to the distance difference ΔR is the flat earth phase, which can be described as follows:

$$\phi_f = -\frac{4\pi}{\lambda}(S_2P - S_1P) = -\frac{4\pi}{\lambda}\Delta R, \tag{3}$$

where S_2P indicates the distance between the aperture S_2 and the target point P, and S_1P is the distance between the aperture S_1 and P. Based on the orbital parameters from the head file and the geographic coordinates of reference points from a geographical reference file, the geocentric coordinates of S_1, S_2 and P can be obtained as described below (Cao et al., 2013).

(1) The aperture position $S(x,y,z)$ when the target is being imaged

First, based on its row and column number (m_P, n_P) in the original satellite data, the imaging time of P point is given by

$$t_P = t_s + \frac{m_P - 1}{PRF} + \frac{n_P - 1}{2RSF}, \tag{4}$$

where t_s indicates the imaging time of the first resolution unit, and PRF and RSF indicate the pulse repetition frequency and the range sampling frequency, respectively.

Second, the orbit equation, $x(t)$, $y(t)$ and $z(t)$, is fitted based on the orbit information from the head file.

$$\left.\begin{aligned} x(t) &= a_0 + a_1 t + a_2 t^2 + a_3 t^3 \\ y(t) &= b_0 + b_1 t + b_2 t^2 + b_3 t^3 \\ z(t) &= c_0 + c_1 t + c_2 t^2 + c_3 t^3 \end{aligned}\right\}, \tag{5}$$

where x, y and z are the orbit coordinates, a_i, b_i and c_i (i = 0, 1, 2, 3) are the fitting coefficients, and t is the time variable. Equation (5) describes the change of the orbit coordinates with time. Then, the aperture position $S(x,y,z)$ as the point P is being imaged can be obtained by substituting the imaging time (t_P) of point P into Eq. (5). Note that the positions of the two satellites in formation need to be calculated, respectively.

(2) The target position $P(x_P, y_P, z_P)$ in the geocentric coordinate system

First, the latitude (*lat*) and longitude (*lon*) are fitted as a function of the row number (m) and column number (n) based on the location information from the geographical reference file.

$$\left.\begin{aligned} lat &= \alpha_0 + \alpha_1 m + \alpha_2 n + \alpha_3 m^2 + \alpha_4 n^2 + \alpha_5 mn \\ lon &= \beta_0 + \beta_1 m + \beta_2 n + \beta_3 m^2 + \beta_4 n^2 + \beta_5 mn \end{aligned}\right\}, \tag{6}$$

where α_i and β_i (i = 0, 1, 2, 3, 4, 5) are the fitting coefficients. Then, the latitude and longitude of point P can be obtained by substituting the row and column number (m_P, n_P) of point P into Eq. (6).

Second, the latitude and longitude of point P are transformed to geocentric coordinates using the following formula:

$$\left.\begin{aligned} N &= a/\sqrt{1 - e \cdot (\sin(lat))^2} \\ x_P &= N \cdot \cos(lat) \cdot \cos(lon) \\ y_P &= N \cdot \cos(lat) \cdot \sin(lon) \\ z_P &= (N - N \cdot e) \cdot \sin(lat) \end{aligned}\right\}, \tag{7}$$

where a, b and e indicate the long axis, short axis and eccentricity of the WGS84 ellipsoid, respectively.

3.3 *Comparison and analysis of conventional methods*

The original interferogram from the ATI complex data introduced in Section 2 is shown in Fig. 2. Note that the data are presented in image coordinates, the radar look direction (i.e., the range direction) is exactly from left to right in the figures. The phase changes periodically during the interval (–π, π] along the range and azimuth directions; this phase change is caused primarily by the flat earth effect. The flat earth phase obscures the ocean surface current information; thus it should be removed. Here, the conventional frequency shift method and the orbital parameters method are used to remove the flat earth effect, respectively. The result is shown in Fig. 3, where it can be found that, although there is phase wrapping (mainly caused by the ocean surface current), the periodic fringes have been removed by the two methods, indicating that both methods have removed the flat earth phase. Nevertheless, the methods' performances are quite different; the orbital parameters method accurately and effectively removes the flat earth phase based on the precise orbit parameters of the TerraSAR-X satellite (Werninghaus and Buckreuss, 2010; Yoon et al., 2009); however, a large amount of residual flat earth phase remains in the frequency shift method result. In the ideal case (i.e., a zero across-track baseline), ATI-SAR detects only the ocean surface velocity field. Because the movement speed is zero over the land or island regions, the absolute value of the calibrated interferometric phase should also be zero. When no phase calibration is conducted, the phase relative value after flat earth phase removal generally has an offset from zero, but it tends to be homogeneous (i.e., the phase variation should be small). In contrast, in the actual results shown in Fig. 3a, the phase variation across different land

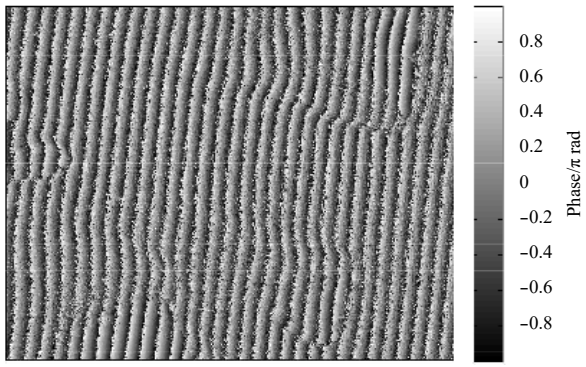

Fig. 2. The original interferometric phase. The radar look direction is from left to right (the unit is π rad, the same as below).

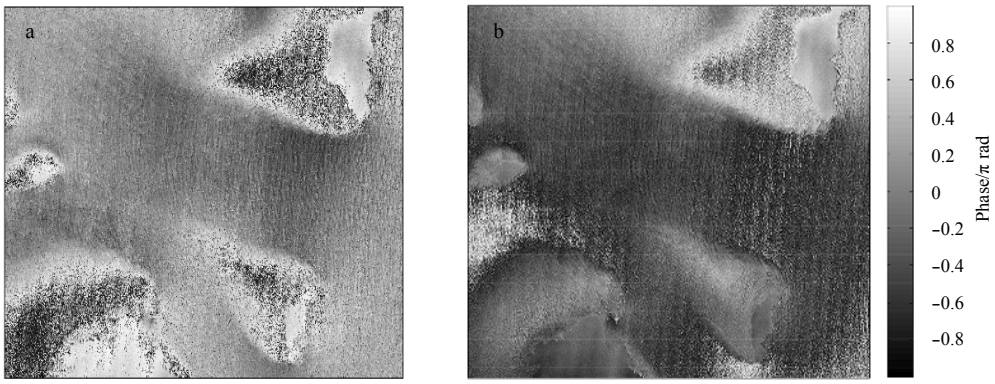

Fig. 3. The relative interferometric phase after removing the flat earth effect. a. Orbital parameters method and b. conventional frequency shift method.

masses and islands is small, indicating that the orbital parameters method accurately removed the flat earth phase. However, the phase variation is significant across the various islands in Fig. 3b, indicating that a large amount of residual flat earth phase remains in the result after applying the frequency shift method.

To present our argument more clearly, the unwrapped phase calibrated by averaging the land region phase to zero, which is the absolute value of the interference phase, is shown in Fig. 4. In Fig. 4a, the orbital parameters method causes the phase over land masses and islands to all tend toward zero; and the little remaining phase variations can be attributed primarily to scattered noise and topological fluctuations. However, in the frequency shift method results shown in Fig. 4b, the phases of several islands deviate significantly from zero. For example, the phase of the land at the lower left is less than zero, while that of the upper right island is greater than zero. Overall, the orbital parameters method accurately removes the flat earth phase, while the frequency shift method leaves a large amount of residual flat earth phase. In the following section, an improved method will be proposed for the frequency shift method that removes the residual flat earth phase.

4 Improved method and discussion

4.1 *Improved frequency shift method based on the ATI-SAR phase feature*

The improved frequency shift method is conducted using the following steps.

(1) Divide the phase diagram into sub-blocks to calculate the frequency spectrum peak value of phase fringes.

In an actual ATI interferogram shown in Fig. 2, the spatial frequency of the phase fringes is generally not a constant; instead, it varies slowly along the range direction. In the conventional frequency shift method described above, the frequency spectrum peak value is the average spatial frequency of the phase fringe over the entire image and does not consider variations in spatial frequency with position. This omission results in obvious errors of flat earth phase removal at both ends of the range direction. To account for the variations of fringe spatial frequency, we divide the interferogram into several sub-blocks to calculate the spatial frequency of the phase fringes. Using this approach, we can not only improve the precision but also obtain its spatial variation.

First, we divide the interferogram into several sub-blocks along the range direction and calculate the frequency spectrum peak value f of each block using the first step of the conventional frequency shift method. The number of sub-blocks is governed by two contradictory factors. On one hand, in principle, the larger the number of sub-blocks is, the more distinct the spatial frequency variations are. On the other hand, if the number of sub-blocks is too large, the length of each sub-block in the range direction will be too small, which makes calculating the spatial frequency accurately a challenge. Although the periodical variations from $-\pi$ to π of the original interference phase are mainly caused by the flat earth effect, as shown in Fig. 2, ocean surface currents and wave motion also affects the spatial distribution of the phase fringes—the distribution of phase fringe is especially distorted in regions with large velocity gradients. These distortions directly affect the spatial frequency estimation of the phase

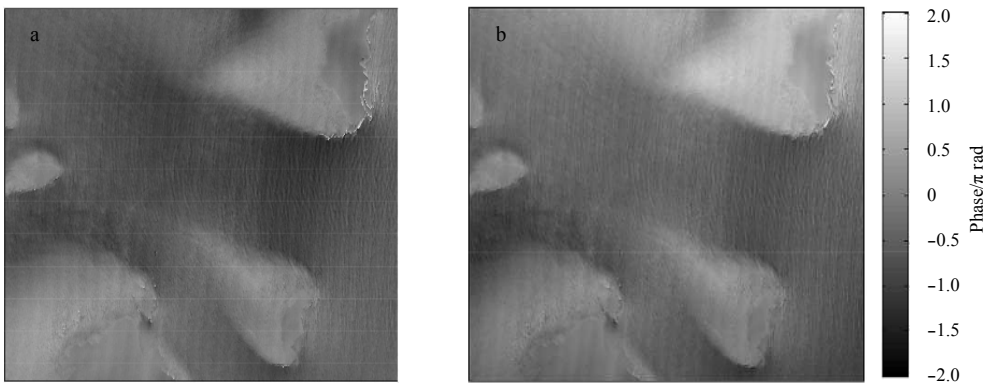

Fig. 4. The unwrapped absolute phase. a. Orbital parameters method and b. conventional frequency shift method.

fringes. The smaller the sub-block size is, the more serious the influence of phase fringe distortion is. To suppress this effect, the length of each phase diagram sub-block in the range direction should be larger than several spatial periods, and abnormal spatial frequency values should be discarded. Based on the above principles, while also considering that the following second-order polynomial fitting requires a minimum of 3 sub-blocks, we divide the phase diagram into five sub-blocks.

Second, we fit the second-order functional relationship between the spatial frequency f and the position n of the center point of each sub-block in the range direction.

$$f(n) = a_0 + a_1 n + a_2 n^2, \tag{8}$$

where a_i (i=0, 1, 2) are the fitting coefficients.

Finally, we calculate the frequency spectrum peak value in each grid point using Eq. (8) and then remove the flat earth effect through the second step of the conventional frequency shift method.

The phase after removing flat earth effect by dividing the phase diagram into sub-blocks is shown in Fig. 5. Figure 5a shows the relative phase after removing the flat earth effect, while Fig. 5b shows the relative phase after further unwrapping. It is found that, compared with the conventional frequency shift method, the initial improvement to the method from dividing the phase diagram into sub-blocks significantly suppresses the phase spatial variation in the land regions, indicating that the improvement significantly reduces the residual flat earth phase. However, land region phase still varies to a certain extent among the various spatial positions. This remaining variation can be attributed to two factors if random phase noise is not considered. One factor is residual flat earth phase, which causes the phases of different islands over large distances to vary with the spatial position in both the range and azimuth directions (e.g., the phase of the island in the upper right of Fig. 6a is greater than zero, while the land region in the lower left is less than zero). Therefore, further removal of the residual flat earth phase is needed. The other factor is the effect of topography. In the actual TanDEM-X satellites formation, both AT baseline and XT baseline (24 m in our data) occur; thus, the interferometric phase will be affected by topography. To observe the effect of topography, the phases of the land and island regions from Fig. 5b are shown in Fig. 6. Note that the phase of the island in the upper right corner of Fig. 6a has obvious spatial variations caused primarily by topography rather than by residual flat earth phase because areas as small as this island should result in a homogeneous residual flat earth phase. Thus, topography should also be considered to further remove residual flat earth phase.

(2) Correct the residual flat earth phase by fitting the function between the phase and position of land areas.

Regardless of random phase noise, the spatial variation of the residual flat earth phase should be slow and regular. Therefore, by fitting the function of the phase of the land region to the location coordinates, the residual flat earth phase can be further removed. Note that the effect of topography fluctuations also needs to be avoided or suppressed. Because the wrapped phase may jump from π to –π, which is not convenient for processing, subsequent processing operates on the unwrapped phase (Fig. 5b).

First, we remove the high elevation region of the island, where the phase is seriously affected by the topography. Then, the phase variation in the remaining land region can be considered to be caused only by residual flat earth phase. In Fig. 6a,

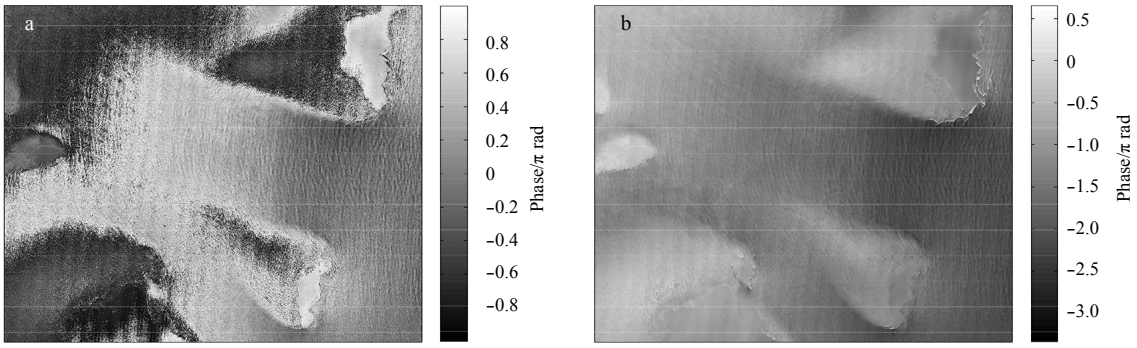

Fig. 5. The relative phase after removing flat earth effect by dividing the phase diagram into five sub-blocks after removing the flat earth effect (a) and after further unwrapping (b).

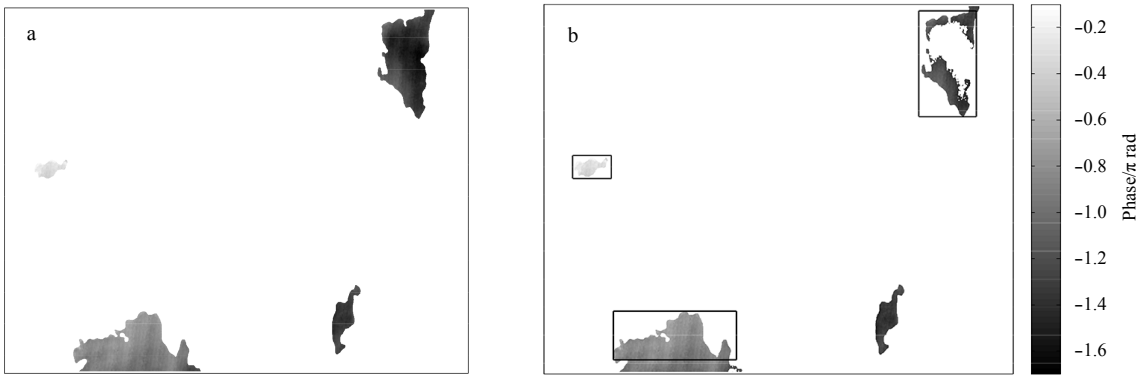

Fig. 6. The phases of land and islands.

the phase of the island in the upper right corner is seriously affected by the island's topography (the elevation varies from 1 m to approximately 50 m and the corresponding phase varies from approximately 1.0π to approximately 1.6π). The elevated areas above 25 m are removed using an ATI phase threshold, and the results are shown in Fig. 6b. The ATI phase threshold is selected not only to suppress the topographical impact but also to ensure that a sufficiently large area remains for phase averaging to remove the random phase noise.

Second, the three island regions (indicated by the black boxes in Fig. 6b) are selected to calibrate the phase. Because each selected area is small, the residual flat earth of each area is approximately constant. Therefore, by averaging the phase of each region and fitting the function between the average phase and the center position of each region, the residual flat earth phase can be further removed. Note that the average phase contains two parts. One is the overall offset of the phase relative value, which does not vary with the position. The other is the residual flat earth phase, which slowly varies with position. A binary linear equation is used to fit the function between the phase correction and position due to the slow change of the residual flat earth phase.

$$\varphi_r(m, n) = b_0 + b_1 m + b_2 n, \tag{9}$$

where b_i (i = 0, 1, 2) are the fitting coefficients, and m and n indicate the row and column number, respectively.

Finally, we calculate the phase correction of every grid point using Eq. (9) and subtract the results from the results of the preliminarily improved method. The calibrated phase is shown in Fig. 7.

4.2 *Comparison and analysis of the improved frequency shift method*

The calibrated phase obtained through the improved frequency shift method is shown in Fig. 7. As shown, in the land and island regions, the phase tends to be zero with little fluctuation, which indicates that the improved frequency shift method accurately removes the flat earth effect. To further verify the effect of the improved method, the results of the conventional and the improved frequency shift methods are statistically compared with those of the orbital parameters method. Under conditions where accurate orbital parameters and geographic information are provided by TanDEM-X L1B data, the orbital parameters method is considered to be reasonably accurate; in other words, its errors when removing the flat earth phase can be ignored. Scatter

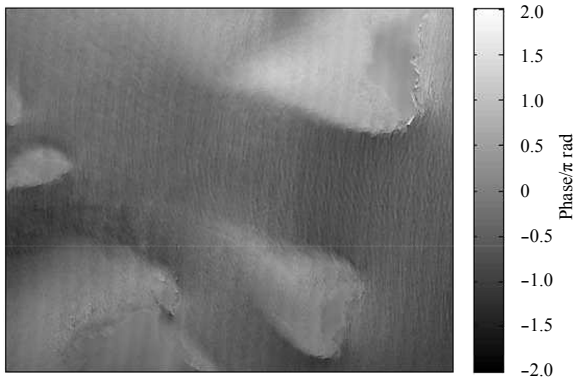

Fig. 7. The calibrated phase obtained with the improved frequency shift method.

diagrams and statistical analysis results are shown in Fig. 8. We computed the shown correlation and regression coefficients, the mean differences, and the residual root mean square (RMS) differences (i.e., the RMS differences after subtracting the mean differences). The results show that a large difference exists between the conventional frequency shift method and the orbital parameters method; this difference occurs because the conventional phase-shift method still retains a large number of unevenly distributed residual flat earth phase. In contrast, the improved frequency shift method agrees well with the orbital parameters method; the correlation coefficient and the regression coefficient are 0.984 and 1.031, respectively, which are great improvements from 0.824 and 0.531 values respectively achieved by the conventional frequency shift method. The accuracy is also greatly improved, the average difference decreases from –0.22π to –0.03π, and the root mean square error decreases from 0.44π to 0.11π. These reductions indicate that the accuracy of the improved method is similar to that of the orbital parameters method.

In view of the above analysis, the orbital parameters method may be the first choice for ATI-SAR flat earth phase removal. When sufficiently accurate orbital parameters are available, the orbital parameters method can accurately remove the flat earth phase. However, for some satellites, the orbital parameters are relatively inaccurate causing the orbital parameters method to have low accuracy when removing the flat-earth phase. In particular, when the orbital parameters are unavailable, the method cannot be used. In such cases, the improved frequency shift method proposed in this paper is an alternative for removing the

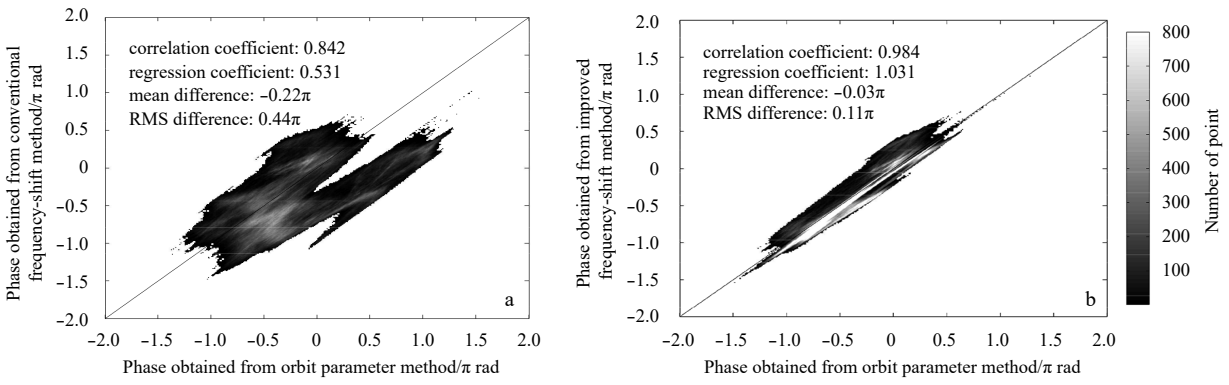

Fig. 8. Scatter diagrams of absolute phase. a. Conventional frequency shift method versus orbital parameters method, and b. improved frequency shift method versus orbital parameters method.

flat-earth phase. The improved frequency shift method achieves approximately the same accuracy for flat earth phase removal as the orbital parameters method when the accurate parameters are available; however, the improved frequency shift method is based solely on the interferogram and does not require any additional parameters.

5 Conclusions

In this paper, various approaches to removing the flat earth phase from ATI-SAR images are investigated. First, the conventional frequency shift and orbital parameters method are introduced, and the effects of the two methods are compared using along-track interferometric data. We found that while the orbital parameters method accurately and effectively removes the flat earth phase when precise satellite orbital parameters (in this case, TanDEM-X) are available; however, the conventional frequency shift method results retained a large amount of residual flat earth phase. To improve the accuracy of the frequency shift method, the spatial frequency of the phase fringe is calculated by dividing the phase diagram into five sub-blocks. Based on the ATI phase characteristic that land region phase tends toward zero, the residual flat earth phase is further corrected by fitting a function between the land area phase and position. The results achieved by the improved and conventional frequency shift method are then compared with those by the orbital parameters method, respectively. It is found that the improved frequency shift method proposed in this paper greatly improves the effect of flat earth effect removal. The result of the improved method is good agreement with the orbital parameter method, and the accuracy of the improved method is similar to that of the orbital parameters method.

Acknowledgements

We thank German Aerospace Center (DLR) for providing the TanDEM-X formation ATI data.

References

Ai Bin, Li Xia. 2009. An analysis of different InSAR flattening algorithms and their influence on DEM accuracy. Remote Sensing for Land & Resources (in Chinese), 21(3): 12–18

Bamler R, Hartl P. 1998. Synthetic aperture radar interferometry. Inverse Problems, 14(4): R1–R54, doi: 10.1088/0266-5611/14/4/001

Cao Yongxing, Fan Zhong, Chen Yan, et al. 2013. Flat earth removal and baseline estimation based on orbit parameters using Radarsat-2 image. In: Proceedings of 2013 IEEE Proceedings of the Geoscience and Remote Sensing Symposium. Melbourne, VIC, Australia: IEEE, 346–349

Gatelli F, Guamieri A M, Parizzi F, et al. 1994. The wavenumber shift in SAR interferometry. IEEE Transactions on Geoscience and Remote Sensing, 32(4): 855–865, doi: 10.1109/36.298013

Geudtner D, Schwäbisch M. 1996. An algorithm for precise reconstruction of InSAR imaging geometry: application to "Flat-Earth" phase removal, phase-to-height conversion and geocoding of InSAR-derived DEMs. In: Proceedings of the EUSAR'96-Konferenz. Königswinter, Germany: EUSAR, 249–252

Kimura H, Todo M. 1997. Baseline estimation using ground points for interferometric SAR. In: Proceedings of 1997 IEEE International Geoscience and Remote Sensing Symposium Proceedings. Remote Sensing—A Scientific Vision for Sustainable Development. Singapore, Singapore: IEEE, 442–444

Kohlhase A O, Feigl K L, Massonnet D. 2003. Applying differential InSAR to orbital dynamics: a new approach for estimating ERS trajectories. Journal of Geodesy, 77(9): 493–502, doi: 10.1007/s00190-003-0336-3

Krieger G, Moreira A, Fiedler H, et al. 2007. TanDEM-X: a satellite formation for high-resolution SAR interferometry. IEEE Transactions on Geoscience and Remote Sensing, 45(11): 3317–3341, doi: 10.1109/TGRS.2007.900693

Moreira J, Schwabisch M, Fornaro G, et al. 1995. X-SAR interferometry: first results. IEEE Transactions on Geoscience and Remote Sensing, 33(4): 950–956, doi: 10.1109/36.406681

Peng S R, He K X, Wang Y N, et al. 2009. A high accurate approach for InSAR flat earth effect removal. In: Proceedings of 2009 International Conference on Measuring Technology and Mechatronics Automation. Zhangjiajie, Hunan, China: IEEE, 742–745

Romeiser R, Runge H, Suchandt S, et al. 2014. Quality assessment of surface current fields from TerraSAR-X and TanDEM-X along-track interferometry and Doppler centroid analysis. IEEE Transactions on Geoscience and Remote Sensing, 52(5): 2759–2772, doi: 10.1109/TGRS.2013.2265659

Romeiser R, Suchandt S, Runge H, et al. 2010. First analysis of TerraSAR-X along-track InSAR-derived current fields. IEEE Transactions on Geoscience and Remote Sensing, 48(2): 820–829, doi: 10.1109/TGRS.2009.2030885

Rosen P A, Hensley S, Joughin I R, et al. 2000. Synthetic aperture radar interferometry. Proceedings of the IEEE, 88(3): 333–382, doi: 10.1109/5.838084

Stangl M, Werninghaus R, Schweizer B, et al. 2006. TerraSAR-X technologies and first results. IEE Proceedings-Radar, Sonar and Navigation, 153(2): 86–95, doi: 10.1049/ip-rsn:20045119

Suchandt S, Runge H. 2015. Ocean surface observations using the TanDEM-X satellite formation. IEEE Journal of Selected Topics in Applied Earth Observations and Remote Sensing, 8(11): 5096–5105, doi: 10.1109/JSTARS.2015.2446893

Wang Lucai, Wang Yaonan, Dai Yuxing. 2004. An improving algorithm of eliminating the horizontal ground effect of phase interference graph in InSAR imaging. Journal of Natural Science of Hunan Normal University (in Chinese), 27(3): 51–55

Werninghaus R, Buckreuss S. 2010. The TerraSAR-X mission and system design. IEEE Transactions on Geoscience and Remote Sensing, 48(2): 606–614, doi: 10.1109/TGRS.2009.2031062

Yoon Y T, Eineder M, Yague-Martinez N, et al. 2009. TerraSAR-X precise trajectory estimation and quality assessment. IEEE Transactions on Geoscience and Remote Sensing, 47(6): 1859–1868, doi: 10.1109/TGRS.2008.2006983

Zebker H A, Rosen P A, Hensley S. 1997. Atmospheric effects in interferometric synthetic aperture radar surface deformation and topographic maps. Journal of Geophysical Research: Solid Earth, 102(B4): 7547–7563, doi: 10.1029/96JB03804